Journal of Systems Engineering and Electronics
Vol. 33, No. 3, June 2022, pp.511 – 521

Scattering center modeling for low-detectable targets

CHEN Yanxi, GUO Kunyi*, XIAO Guangliang, and SHENG Xinqing

Institute of Radio Frequency Technology and Software, School of Integrated Circuits and Electronics, Beijing Institute of Technology, Beijing 100081, China

Abstract: The scattering centers (SCs) of low-detectable targets (LDTs) have a low scattering intensity. It is difficult to build the SC model of an LDT using the existing methods because these methods mainly concern dominant SCs with strong scattering contributions. This paper presents an SC modeling approach to acquire the weak SCs of LDTs. We employ the induced currents at the LDT to search SCs, and the joint time-frequency transform together with the Hough transform to separate the scattering contributions of different SCs. Particle swarm optimization (PSO) is applied to improve the estimation results of SCs. The accuracy of the SC model built by this approach is verified by a full-wave numerical method. The validation results show that the SC model of the LDT can precisely simulate the signatures of high-resolution images, such as high-resolution range profile and inverse synthetic aperture radar (ISAR) images.

Keywords: low-detectable target (LDT), stealth target, scattering center (SC) model, time-frequency representation, full-wave method.

DOI: 10.23919/JSEE.2022.000051

1. Introduction

Low-detectable targets (LDTs) have much lower radar cross section (RCS) than general radar targets under some of the most frequently employed observation angles, which makes them difficult to be captured by radar. Low scattering intensity of LDTs depend on two techniques: stealth shape design and absorbent material coating. An LDT with a designed stealth shape is considered in this paper. The stealth shape makes the radar echoes from the LDT mainly consist of weak scattering contributions, such as diffracted waves from geometry discontinuities and creeping or traveling waves along smooth surfaces. More seriously, for streamlined stealth aircraft, the geometric discontinuities are mainly concentrated in the lips of the inlet and the tail nozzle, where the wings and the fuselage are connected. Therefore, stealth aircraft commonly have weak, nearly distributed scattering centers (SCs). The locations of the SCs are difficult to be determined, and their parameters are difficult to be extracted from the scattering field of LDTs.

SC models developed for complex targets have attracted much attention in the field of radar detection [1]. SC models have been well demonstrated to be capable of describing the complex scattering characteristics of a target by using a physically relevant yet concise model [2−4]. The existing methods of SC modeling generally include two parts: choosing suitable analytical models (with unknowns that need to be determined) to describe the scattering contributions of the SCs and acquiring the parameters of the SC model from the scattered fields of the target or the imaging results of the scattered fields. These analytical models are generally derived from the high-frequency approximate solutions of canonical geometric structures [5−7]. High-frequency methods include the method of physical optics (PO), the geometrical theory of diffraction (GTD) and the method of equivalent edge current (EEC).

The existing methods for parameter extraction include forward methods and inverse methods. In forward methods, the scattering contribution of each SC is obtained by electromagnetic calculations, such as the method of using high-frequency methods [8] and another that utilizes equivalent currents computed by the full-wave method [9]. In inverse methods, the SC parameters are mainly extracted from the scattering fields of the target or the imaging results by parameter estimation, such as the CLEAN method [10], maximum likelihood estimation [11], support vector machine [12], genetic algorithm (GA) and particle swarm optimization (PSO) [13−15].

Dominant scattering contributions, such as reflection by a smooth surface with a large size and diffraction by a straight or curved edge with a large curvature, can be well described by the solutions of high-frequency methods. However, the scattering waves of LDTs are mainly contributed by weak scattering mechanisms, e.g., diffractions by irregular geometrical discontinuities. The scatter-

Manuscript received December 22, 2020.
*Corresponding author.
This work was supported by the National Key R&D Program of China (2017YFB0202500), and the National Natural Science Foundation of China (61771052).

ing characteristics of irregular geometrical structures are different from those of canonical geometric structures. The SC models derived from canonical geometric structures cannot be directly applied to LDTs and need to be modified according to the scattering characteristics of LDTs. In addition, the distances among the weak SCs are too close to be resolved in the imaging results. These reasons make it difficult to obtain highly accurate SC models by using existing parameter extraction methods.

To address this problem, this paper presents several more suitable SC models and an improved method of SC modeling for LDTs. The improvement includes the following aspects: First, the mathematical models of the weak SCs of LDTs are modified according to their real scattering characteristics. Second, the locations of the weak SCs are determined by using a combined joint time-frequency transform (JTFT), the sinusoidal Hough transform, and the induced current analysis. Third, in the process of parameter estimation, objective functions combining root mean square error (RMSE) and image similarity are selected to improve the estimation precision.

To validate this method, SC models of a stealth aircraft are built, and the high-resolution range profile (HRRP) and inverse synthetic aperture radar (ISAR) images simulated by the SC models are compared with the image results obtained by the full-wave numerical method, i.e., parallel-multilevel fast multiple algorithm (PMLFMA) [16]. The results show that the SC models can precisely describe the signatures of HRRP and ISAR images.

The remainder of this paper is organized as follows: Section 2 presents the scattering characteristic analysis of LDTs; Section 3 presents the improved parametric SC models for weak SCs; Section 4 presents the search method for SCs that are hard to determine; Section 5 presents the improved method of parameter estimation; Section 6 gives the validation of the built SC models; and conclusions of this paper are drawn in Section 7 .

2. Scattering characteristics of LDTs

A stealth aircraft is investigated as an instance of an LDT. The target, the coordinate system, and the light of sight (LOS) of the radar used in this paper are shown in Fig. 1 (a). To clearly show the difference between an LDT and a nonstealth target, an aircraft without a stealth shape design is also considered, as shown in Fig. 1(b).

The monostatic RCS of the stealth aircraft and that of nonstealth aircraft under HH polarization are computed by PMLFMA. The radar frequency is 1.5 GHz, and the observation angle is set as follows: elevation angle θ=90°, azimuth angle ϕ=0°−180°, with a step of 0.1°. To limit the computational complexity of the full-wave method, we seal the inlet with metal plates, but retain the edge structures of the inlet lip. The time costs for the two aircraft are 16.5 h and 13.6 h, respectively. The parameters of the used high-performance server cluster are four 14-core 64-bit Intel Xeon E7-4850 CPUs and 1 TB of RAM. The results are shown in Fig. 2. We can see that the RCS of the stealth aircraft is considerably smaller than that of the nonstealth aircraft, especially within the range of sensitive observation angles.

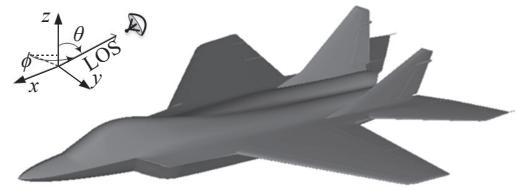

(a) Stealth aircraft

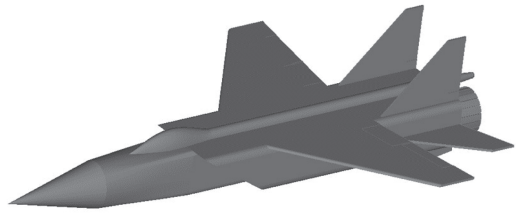

(b) Nonstealth aircraft

Fig. 1 Geometry of aircraft

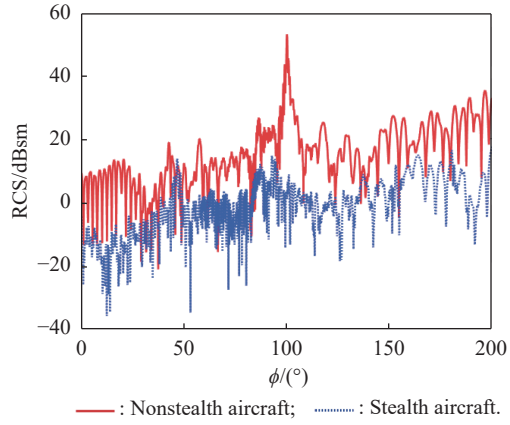

Fig. 2 RCS results of the stealth and the nonstealth aircraft

The single-frequency scattering waves of the target collected at different aspect angles can be converted into the time-frequency representations (TFRs) by JTFT. TFR can show the amplitude and location dependence of an SC on the aspect angle [17]. In addition, different types of SCs have obvious image signatures [18]. Therefore, we analyze the differences in scattering characteristics between the LDT and the nonstealth target through the TFR. The most commonly used JTFT methods in SC modeling include the short-time Fourier transform (STFT), smoothed pseudo-Wigner Ville distribution (SPWVD) and the reassigned SPWVD (RSPWVD) [19,20].

In addition to these three methods, we also use other methods, such as Gabor expansion [21], STFT with fractional Fourier transform (FRFT) [22], continuous wavelet

transform (CWT) [23,24], empirical wavelet transform (EWT) [25], SPWVD with empirical mode decomposition (EMD) [26] and Born-Jordan distribution (BJD) [27]. By comparison, we choose SPWVD to obtain the TFR of scattering waves for LDTs because this method has better resolution than STFT, FRFT-STFT, CWT, and EWT, and less distortion of cross-terms than RSPWVD, EMD-SPWVD and BJD.

The TFR images of the stealth target and the nonstealth target under HH polarization are compared, as shown in Fig. 3. There are four obvious differences between the two TFR images.

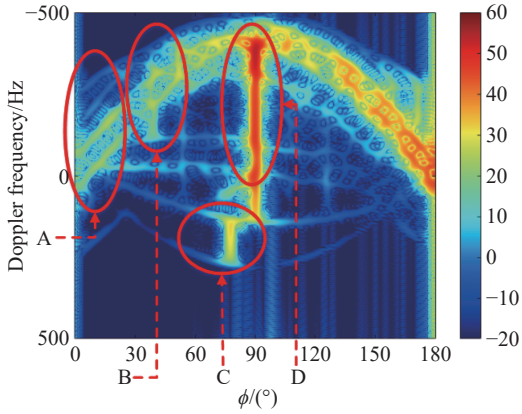

(a) Stealth target

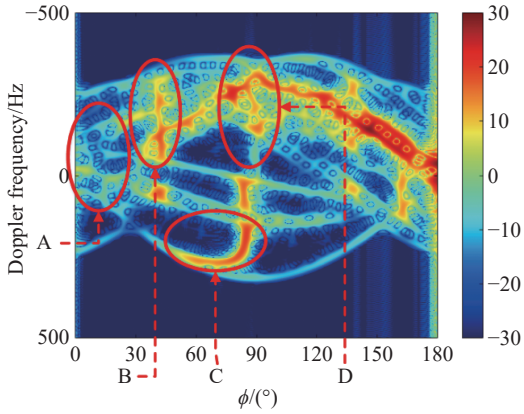

(b) Nonstealth target

Fig. 3 TFRs of the stealth target and the nonstealth target by PMLFMA

For part A: When observing the stealth target within the range of ϕ =0°−25°, the TFR of the stealth target shows that there are no strong SCs but multiple weak SCs. These weak SCs are mainly induced by scattering from the lips of the inlets and are located closely together, which makes it difficult to distinguish them in the TFR. The nonstealth target has only a few SCs, which can be distinguished well. These SCs are induced by the wings parallel to the *Y*-axis.

For part B: For the stealth target, the SCs of the front, rear, and tail wings of the aircraft are distributed SCs (DSCs) and are shown as vertical bright lines in the TFR. They are concentrated at ϕ =42°, because the leading edges of the inlet lip, wings and tailfins are designed in parallel.

For part C: The SC of the nose of the stealth target is a sliding SC (SSC), which is shown as a curve in TFR due to the double-curved surface of the nose. While the nose of the nonstealth target is cone-shaped, the SC of the nose is a DSC; therefore, it appears as a vertical bright line.

For part D: For the stealth target, there are no obvious DSCs on the fuselage, as the nose, the fuselage and wings of the stealth aircraft are designed as a whole streamlined surface. For the nonstealth target, however, the DSC on the cylindrical fuselage and the DSC on the vertical tail are obviously shown at ϕ =90°.

The dominant signatures in the TFR when ϕ >90° are mainly attributed to scattering from the discontinuity of the tail nozzle. The aspect angle ranges of this paper are θ= 85°−95°, ϕ=−70°−70°, therefore these SCs on the discontinuities of the tail nozzle are not considered in the following SC modeling.

According to the above analysis, we know that the SCs of the stealth target that appear within the observation angles of interest for the stealth target are weakly localized SCs (LSCs) on inlet lips and the discontinuities of wings and fuselage, DSCs on the front and rear edges of wings, and SSCs on the nose.

For non-stealth targets mainly composed of planes, the main scattering centers have strong amplitudes and are far apart, so they are easy to determine. For example, the position of the SC can be automatically detected by the ray tracing method [8], or manually marked by observing the computer aided design model [28]. Due to the complexity of the geometrical structures of the stealth target, the locations of these SCs are difficult to determine by using the traditional methods above. The whole computation time is too long to be realized.

In this paper, we use a series of improved methods to acquire the locations of the SCs of the stealth aircraft. No more computations than the traditional methods are involved. In addition, to acquire high-precision SC parameters, further improvements of the parameter estimation method is introduced in Section 5.

3. Improved SC models for the LDT

The following types of SCs exist for the stealth aircraft within the aspect angle range of interest: LSCs induced by diffraction from vertexes and the intersection points of the edge and surface (denoted by LSC-V and LSC-I), SSCs induced by diffraction of irregular curved edges formed by the intersection of surfaces (SSC-E) and reflection of streamlined surfaces (SSC-S), DSCs induced by diffraction from straight edges and the rounded leading

edges of the wings (denoted by DSC-D), and DSCs induced by reflection from single-curved surfaces of the fuselage (denoted by DSC-R).

DSC-Rs commonly have stronger scattering amplitudes than other types of SCs, but their amount is less in stealth aircraft. Therefore, the main SC types that determine the scattering characteristics of stealth aircraft are LSCs, SSC-Es, and DSC-Ds. For LSCs and SSC-Es, there are no closed-form solutions for the diffraction of these irregular discontinuities. Therefore, we extract the mathematical model of the weak SCs, through fitting the scattering field data. For DSC-Ds, we modify the commonly used DSC model to make it more suitable for the scattering mechanism of the leading edges.

To obtain the 3D SC model, we first estimate the parameters of the SC model at a given elevation angle of θ_n, within the range of 85°−95° and the changed azimuth angle of ϕ =−70°−70°. Then we obtain the parameters under other elevation angles with the same process.

3.1 LSC

For the LSCs, the commonly used SC model [7] is as follows:

$$E_{\mathrm{LSC}}(f,\phi)=A\left(\frac{\mathrm{j}f}{f_c}\right)^{\alpha}\exp\left(-\gamma\left|\sin(\phi-\bar{\phi})\right|\right)\cdot \exp(\mathrm{j}2k\boldsymbol{r}'\cdot\hat{\boldsymbol{r}}_{\mathrm{los}}) \tag{1}$$

where A is a complex constant and α is the frequency dependence factor, which is an integer multiple of 1/2, and the value of α is related to the geometry that forms the SC [6]; k is the wavenumber; $\boldsymbol{r}'$ is the location vector of the SC; $\hat{\boldsymbol{r}}_{\mathrm{los}}$ is the unit vector of LOS of the radar and it changes in θ_n and ϕ. There are three unknown parameters in the LSC expression that need to be estimated: $A,\bar{\phi}$, and γ.

For the stealth aircraft, there are two types of LSCs, namely, LSC-V and LSC-I, as illustrated in Fig. 4 in red dots and yellow stars, respectively. The scattering fields of the LSCs are computed by the currents near the vertex and interaction points [9], as shown in Fig. 5. We can see that the scattering amplitude of LSC-V hardly changes with the elevation angle and decreases monotonically with the elevation angle, which agrees with the form of the exponential function in (1). However, unlike LSC-V, the scattering amplitude of LSC-I changes in both the elevation angle and the azimuth angle.

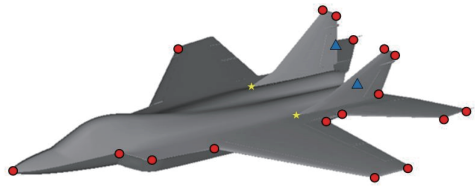

Fig. 4 Location of the main LSCs of the stealth target

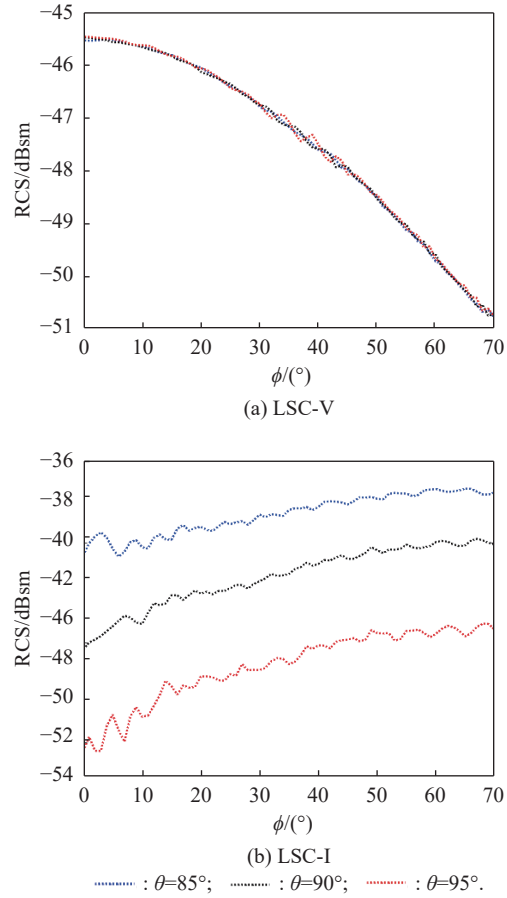

Fig. 5 Change in the scattering amplitude of LSC-V and LSC-I with aspect angle

Considering the aspect dependence of the LSC-I, we use the following 3D model to describe the scattering characteristics:

$$E_{\mathrm{LSC}}(f,\theta_n,\phi)=A_n^L\left(\frac{\mathrm{j}f}{f_c}\right)^{\alpha}W(\phi-\bar{\phi}_n)\cdot \exp\left(-\gamma_n\left|\sin(\phi-\bar{\phi}_n)\right|\right)\exp(\mathrm{j}2k\boldsymbol{r}'\cdot\hat{\boldsymbol{r}}_{\mathrm{los}}), \tag{2}$$

$$A_n^L=\begin{cases}C_0, & \text{for LSC-V}\\ C_1\sin(C_2\theta_n+C_3), & \text{for LSC-I}\end{cases}, \tag{3}$$

where W is the Hamming window function. θ_n is the nth elevation angle; C_0, C_1, C_2, C_3, $\bar{\phi}_n$, and γ_n are the parameters under a given θ_n. They are invariant with ϕ and need to be estimated.

3.2 SSC

The SSCs of the stealth aircraft under the given aspect angle are illustrated in Fig. 6 as red lines. Among them, the SSC-E formed by the reflection of the rounded curved edge on the nose shows an obvious feature in the TFR as

shown in Fig. 3(a) (part C). It is the most important SSC of the streamlined target; it appears at ϕ =0°−70°, and slides on the edge with the change in the LOS of the radar.

Fig. 6 Location of the main SSCs of the stealth target

According to the geometry of the nose, we easily extract the location of the SSC-E according to the normal direction of the surface. After obtaining the position function, the scattering amplitude can be extracted from the TFR if the image signature of the SSC-E is distinguishable. The amplitude function extracted directly from the TFR is given in Fig. 7.

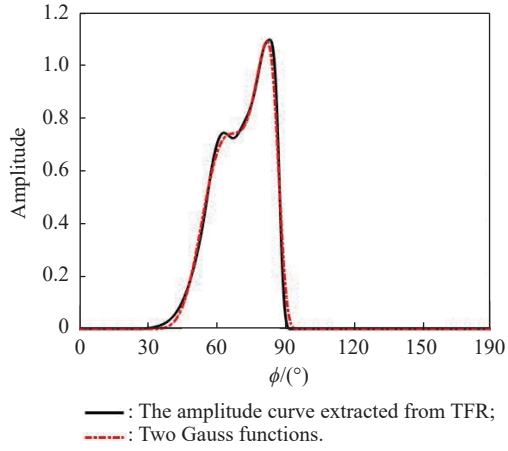

Fig. 7 Amplitude curve of the SSC on the head of the stealth target

We can see that the change in amplitude can be divided into two sections. We apply the sum of two simple Gauss functions to describe the change in amplitude, which can be given by

$$E_{\mathrm{SSC}}(f,\theta_n,\phi)=A_n^S(\phi)\left(\frac{\mathrm{j}f}{f_c}\right)^{\alpha}\cdot \exp\left(\mathrm{j}2k(\boldsymbol{r}_i(\theta_n,\phi)\cdot\hat{\boldsymbol{r}}_{\mathrm{los}})\right), \tag{4}$$

$$A_n^S(\phi)=\begin{cases} C_0, & \text{for SSC-S with small visible angle} \\ C_1\exp(\alpha_1(\sin(\phi-\beta_1))^2)+ & \\ \quad C_2\exp(\alpha_2(\sin(\phi-\beta_2))^2), & \text{for SSC-E} \end{cases}, \tag{5}$$

where $A_n^S(\phi)$ is a function of amplitude; C_0, C_1, C_2, α_1, α_2, β_1, and β_2 are parameters that need to be estimated; $\boldsymbol{r}_i(\theta_n,\phi)$ describes the position vector of the SSC, which changes with θ_n and ϕ. This model is more concise than the commonly used rational polynomial function [29], so it is more conducive to the subsequent parameter estimation.

3.3 DSC

For the DSCs, the commonly used 2D DSC model is derived from the PO solution of the planar surface [7], which can be expressed as follows:

$$E_{\mathrm{DSC}}(f,\phi)=A\left(\frac{\mathrm{j}f}{f_c}\right)^{\alpha}\mathrm{sinc}\left(kL\sin(\phi-\bar{\phi})\right)\cdot \exp\left(\mathrm{j}2k\boldsymbol{r}'\cdot\hat{\boldsymbol{r}}_{\mathrm{los}}\right) \tag{6}$$

where L is the distribution length of the DSC.

The DSCs of the stealth aircraft are mainly located at the edges of the wings and fuselage, as shown in Fig. 8. These edges are actually cylindrical or conical surfaces with a certain curvature radius. For example, the curvature radius of the leading edge of the side wing is approximately 22 mm. Therefore, we modify (6) according to the scattering by a conical surface.

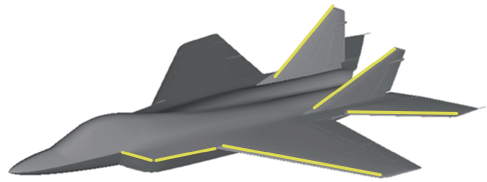

Fig. 8 Location of the main DSCs of the stealth target

According to the PO solution of the conical surface, the model for this DSC-D is expressed as follows:

$$E_{\mathrm{DSC-D}}(f,\theta_n,\phi)=A_n\left(\frac{\mathrm{j}f}{f_c}\right)^{\alpha}\cos(\phi-\bar{\phi}_n)\cdot \mathrm{sinc}\left(kL\sin(\phi-\bar{\phi}_n)\right)\exp\left(\mathrm{j}2k\boldsymbol{r}'\cdot\hat{\boldsymbol{r}}_{\mathrm{los}}\right) \tag{7}$$

where L is invariant with θ_n, because the length of the leading edge is invariant; A_n, $\bar{\phi}_n$ are parameters need to be estimated. In (7), the leading edge is with the *XOY* plane, therefore the scattering amplitude changes in azimuth angle with the forms of sinc and cos functions [28,30].

Due to the artificial plugging of the cavity at the inlets, there is a DSC-R generated by plane reflection, which can be expressed by the SC formula of an arbitrary polygon plate in [31]. This DSC is artificial, which does not truly exist. Other DSC-Rs generated by the approximate plane are not visible in the observation angles, therefore they are not the focus of this paper.

4. Search method for hard-to-find SCs

In the TFR, the SCs formed by different scattering mecha-

nisms have different image signatures [18]. A DSC appears as a bright vertical line, an SSC (on a smooth surface with a large curvature radius) appears as a highlighted curve and an LSC appears as a sinusoidal line. These features are easily identified in TFR. However, for LSCs that are close to each other, it is difficult to identify them directly from TFR due to image feature aliasing. In addition, for the SCs formed by irregular structures, the image features are also irregular, which makes it difficult to recognize them from TFR. Therefore, in addition to using JTFT, the methods are needed to identify SCs that are not easily identified.

4.1 Search for hard-to-find LSCs

For stealth targets, the SCs that can be observed are mainly LSCs. As shown in Fig. 5, the number of geometric discontinuities for the aircraft is enormous. It is impossible to set an LSC at every discontinuity, which will result in redundancy parameters to be estimated; therefore we need to search which LSCs are visible to reduce the difficulty of parameter estimation. In addition, the LSCs of stealth aircraft are close to each other, which results in serious image feature aliasing and cross-terms, which make them hard to identify. To address this, we apply a sinusoidal Hough transform to search the LSCs from TFR by using their sinusoidal Doppler frequency features.

In the TFR image, the relationship between the Doppler frequency and the location of the SC can be expressed as

$$f_D = \frac{2}{\lambda}\frac{\partial}{\partial t}(\boldsymbol{r}' \cdot \hat{\boldsymbol{r}}_{\text{los}}) \tag{8}$$

where $\boldsymbol{r}'$ is a constant vector and the Euler angle is (θ_0, ϕ_0). If we let $\hat{\boldsymbol{r}}_{\text{los}}$ uniformly rotate in the XOY plane ($\phi=\omega$t, θ=90°), then we can rewrite $\boldsymbol{r}' \cdot \hat{\boldsymbol{r}}_{\text{los}}$ as $x'\cos(\phi-\phi_0)+y'\sin(\phi-\phi_0)$. Therefore, the Doppler frequency can be expressed as

$$f_D = F_0(-x'\sin(\phi-\phi_0)+y'\cos(\phi-\phi_0)) \tag{9}$$

where $F_0=\dfrac{2\omega}{\lambda}$; (x', y') represents the coordinate value of the LSC on the XOY plane.

The Hough transform is used to detect geometric features such as circles or lines in images. Its principle is to transform the problem of image detection into the problem of the maximum value in Hough parameter space by using the duality of image and parameter space. The sinusoidal Hough transform is used to detect sinusoidal features in images. Equation (9) is used for mapping. Each feature point in the image corresponds to a group of (x',y') in the parameter space. After all mapping is completed, the parameter values with high votes are selected.

All geometric discontinuities in the 3D model of the stealth aircraft are detected, and a database is constructed using these location data. We can apply the sinusoidal Hough transform to search (x',y') from the database of geometrical discontinuities. This method facilitates the automated modeling of SCs. The search process includes the following steps:

(i) Using the SPWVD method, a TFR image of the stealth target in the angle ranges of θ=90° and ϕ=0°−70° under HH polarization is obtained, as shown in Fig. 9(a).

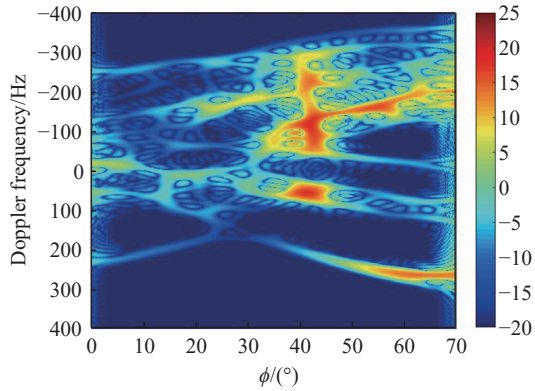

(a) TFR image

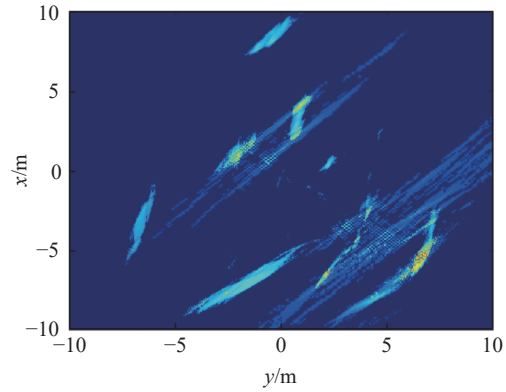

(b) Result of sinusoidal Hough transform

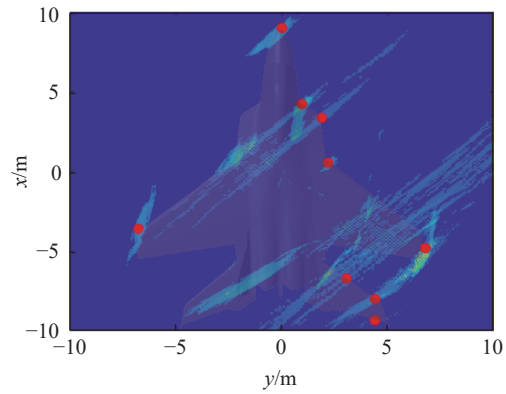

(c) Visible LSCs

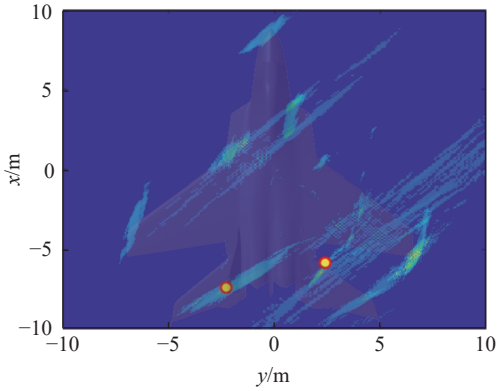

(d) Locations of the LSCs of multiple reflections

Fig. 9 Search process for observable LSCs

(ii) To facilitate the search for sinusoidal features, the TFR image is binarized. The whole image is divided into several small areas appropriately, and a threshold t_1 is set to select valid pixels. The values of points greater than t_1 are considered to be 1, otherwise, they are assumed to be 0. $t_1 = \mu + \delta_1\sigma$, where μ is the mean value of all points in the area; σ is the standard deviation of points; and δ_1 is a constant [32].

(iii) Through the sinusoidal Hough transform, the binarized TFR image is converted into the parameter space, as shown in Fig. 9(b). The highlighted area in the figure indicates that there is a possible LSC.

(iv) The real locations of all geometric discontinuities are compared with the highlighted areas, and a threshold t_2 is set to select the potential LSCs. If the number of votes in the area around an LSC is greater than t_2, it is considered an observable LSC, as displayed with red dots in Fig. 9(c).

In Fig. 9(c), it can be noted that except for all the LSCs from geometric discontinuities, there are more highlighted regions in the parameter space, indicating that there are LSCs but not from geometric discontinuities on the target surface. Based on this, we find two LSCs generated by multiple reflections from the wings of the aircraft. The actual positions are shown by blue triangles in Fig. 5, and their positions in parameter space are shown in Fig. 9(d).

4.2 Determining SCs of small irregular structures

In addition to obvious SCs, there are still some irregular image signatures in the TFR, as shown in Fig. 9(a). They correspond to the scattering from irregular geometrical structures. To search for the hard-to-find geometrical structures that may contribute to the total fields under the observation angles of interest, we apply the induced currents method.

Under the far-field condition, the incident wave can be regarded as a cluster of parallel rays. The induced current intensity of each facet of the target is positively correlated with the area being irradiated. Thus the intensity can be described by the absolute value of the dot product between the incident direction and the normal vector of the lighting area. The induced current intensities of the stealth target under two cases of incident angles (θ=90°, ϕ=0°; θ=90°, ϕ=42.5°) are shown in Fig. 10. The redder color indicates a higher intensity. According to the distribution of the induced current intensity, we can determine the geometrical structures where SCs are easy to be ignored.

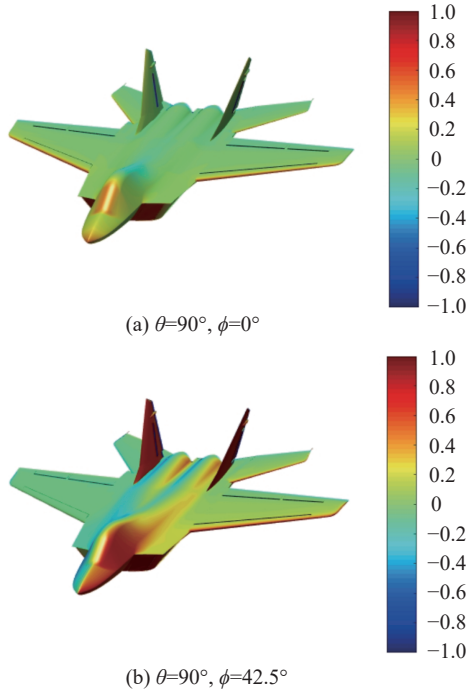

(a) θ=90°, ϕ=0°

(b) θ=90°, ϕ=42.5°

Fig. 10 Induced current intensity on the LDT under different incident angles

For the first case, the main geometrical structures have much weaker induced current intensities, which confirms that the stealth design of this target is effective under the given observation angle. Only the front edges of wings and tails, the regions of inlets, the vertex of the nose and the part of the cabin are much redder than other structures. For the second case, we can see that some of redder areas are distributed on small, irregular geometrical structures, such as the actuator fairing under the wing and the intersection of the cabin and the nose. The strong scattering areas caused by small irregular structures are shown in Fig. 11.

The scattering sources of the air intake port and the actuator fairing are confirmed by the following numerical results, which show that they have a relative strong scattering contribution that needs to be considered in SC modeling. Their corresponding signatures in the TFR are

illustrated in Fig. 12. The scattering characteristics of area A come from the air intake port, and area B come from the actuator fairing. Through observation, these two structures are small-curved surfaces, so they are regarded as two SSCs, which are added to the SC model of the stealth aircraft.

In summary, the complete flow chart of the SC modeling process is shown in Fig. 13.

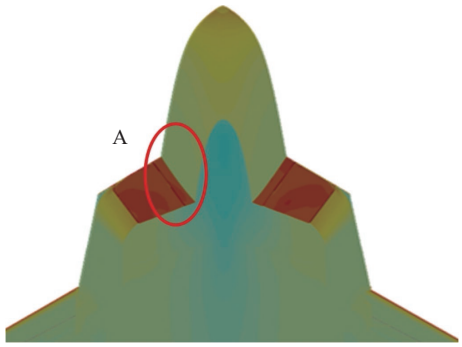

(a) Air intake port

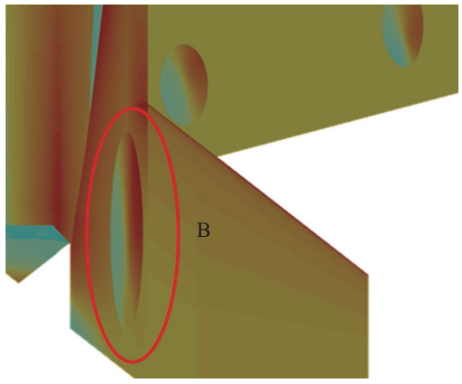

(b) Actuator fairing

Fig. 11 Location of the small structures that produce strong scattering

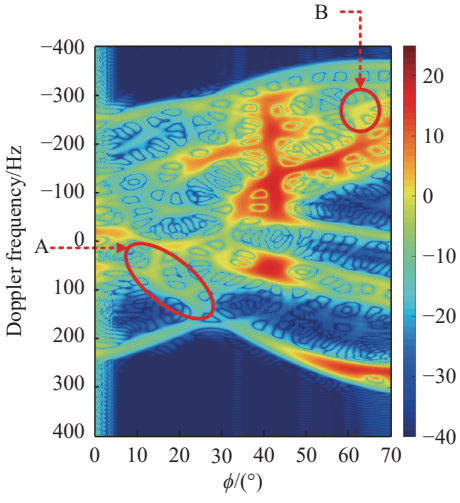

(a) PMLFMA

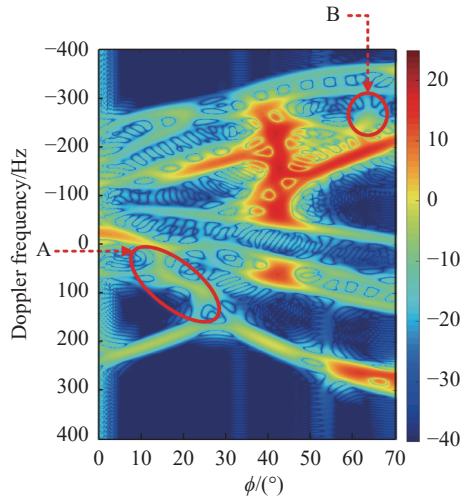

(b) The SC model

Fig. 12 TFR image results of PMLFMA and the SC model

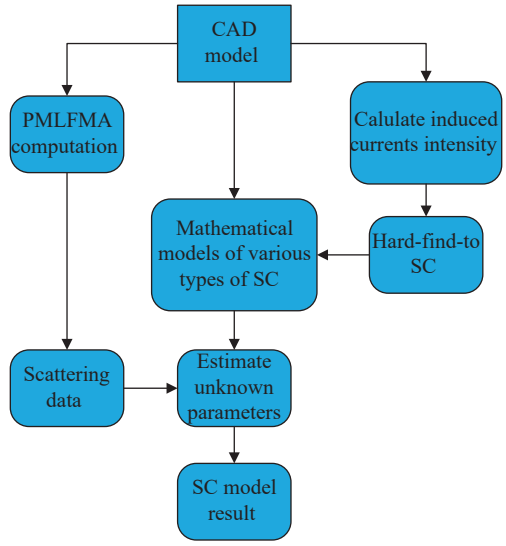

Fig. 13 Flow chart of SC modeling

5. Improved SC parameter estimation method

A large number of parameter optimization methods are currently used to solve engineering problems. The SC model of the stealth aircraft has a large number of parameters that need to be estimated. Therefore, choosing a suitable parameter estimation method and formulating a suitable parameter estimation strategy can improve the modeling efficiency.

Firstly, three representative and commonly used parameter estimation methods are selected for testing: GA, simulated annealing (SA) algorithm, and PSO algorithm. When there are five unknown parameters, the results of GA and PSO are not very different. When there are 100 unknown parameters, the performance of the PSO

algorithm is obviously better, and the performance of the SA algorithm is significantly worse than that of the other two methods. Therefore, the PSO algorithm is chosen to estimate the SC parameters in order to save time when there are many unknowns.

Secondly, when the estimated parameters are too large, the number of iterations of the PSO algorithm greatly increases, and the solution is easily trapped by local optimizations. Therefore, we propose an improved parameter estimation process, which includes three steps:

(i) Through time-frequency analysis, SCs that do not overlap with other SCs can be extracted. The unknown parameters of these SCs can be determined by the linear relationship between the amplitude of the TFR image features and the amplitude of the electric field. By this step, the number of parameters can be reduced afterwards.

(ii) According to the amplitude range of the target's RCS, the upper and lower limits can be determined for the values of the remaining unknown parameters.

(iii) The fitness function of PSO is set to the combination of the TFR image similarity and the RMSE of the RCS when estimating.

To verify the validity of the first and second steps, the parameter estimation of the stealth target SC model is taken as an example, and the TFR image similarity is taken as the fitness function. The comparison results of the estimated time and precision are given in Table 1. The results show that the estimation accuracy is improved and the estimated time is reduced by 64% compared with the case without using the first and second steps.

Table 1 Comparison of parameter estimation efficiency under different conditions

Condition	Similarity of TFR images/%	Number of iterations that tend to converge	Time cost/min
No upper and lower limits, estimate all parameters	82	72	1 008
With upper and lower limits, estimate all parameters	84	30	420
With upper and lower limits, exclude partially identifiable parameters	84	24	360

To verify the validity of the third step, a comparison of the results using different fitness functions to estimate the parameters is given in Table 2. If the combination of the normalized TFR image similarity and the RMSE of RCS is selected as the fitness function, the estimation result is better than the case in which only the RMSE of the RCS is optimized. If the weight of the TFR image similarity is set to two or three times the RMSE of RCS in the fitness function, the number of iterations that tend to converge is further reduced. This is because if only the RMSE of the RCS is optimized, the amplitude parameters of the SCs that overlap satisfy the minimum error but do not conform to the actual amplitude relationship reflected in the TFR image.

Table 2 Comparison of parameter estimation results under different objective functions

Objective function used (normalized)	Similarity of TFR images/%	RMSE of RCS	Number of iterations that tend to converge
A: Similarity of TFR images	84	4.75	24
B: RMSE of RCS	79	4.42	18
A×B	83	4.58	27
A+B	82	4.42	25
2×A+B	82	4.43	20
3×A+B	82	4.44	18

In addition, we compare the performance when using TER images obtained by different JTFT methods to estimate parameters. Through comparison, it is found that the estimation result of the SPWVD method is better than other methods, and the RMSE of RCS is 0.5−3 dB lower.

6. Validation of the SC model by imaging simulation

For the stealth target, 28 SCs (12 DSCs, 12 LSCs, and four SSCs) are used to describe the monostatic scattering waves. According to the above section, the parameters of the SC model are estimated based on the combined objective functions of the RMSE of the RCS and the similarity of the TFR. A comparison of the TFR image between the SC model and the PMLFMA is presented in Fig. 12, and the TFR image similarity between the two is 83%. This section further verifies the precision of the built SC model by the signatures of the HRRP image and the ISAR image.

The HRRP simulated by the model under HH polarization is calculated when θ=90°, ϕ=42°, and the frequency bandwidth is 1 − 1.8 GHz. The comparison of the results of the SC model with the PMLFMA is given in Fig. 14. The HRRP similarity of the two is 98%.

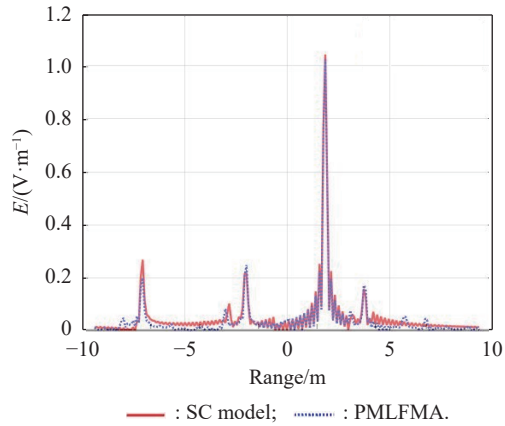

Fig. 14 Results of the HRRP image of the SC model and the PMLFMA under HH polarization

A comparison of the ISAR image results of the PMLFMA and the SC model is shown in Fig. 15. The

calculation parameters of the ISAR image are: f=1 − 2.5 GHz, with a step of 3 MHz, where θ=90° and ϕ=0°−90°, with a step of 0.18°. The ISAR under the wide observation angle range shows the complete contour of the front of the target. The similarity between the ISAR image of the SC model and the full-wave method is 81%, and the contour is basically consistent with the real geometry of the target.

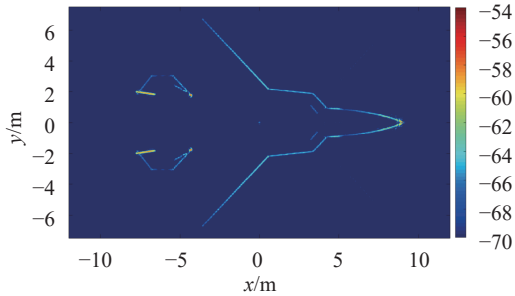

(a) PMLFMA

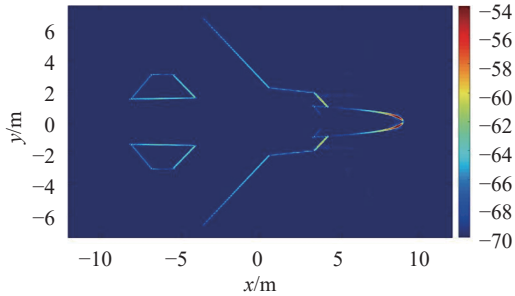

(b) SC model

Fig. 15 Results of ISAR image of PMLFMA and SC model

The SC model is built using only scattering fields under a single frequency. If the high resolution HRRP/ISAR image is obtained by scattering fields under a wide frequency, the SC model can be further improved. In order to further optimize the unknown parameters of the SC model, we use the HRRP results under ϕ=0°, 42°, and 70° to estimate the parameters, the objective function is the sum of the three HRRP image similarities. The ISAR image of the SC model with improved parameters is presented in Fig. 16, and the similarity between the ISAR image of the improved SC model and the full-wave method is 85%.

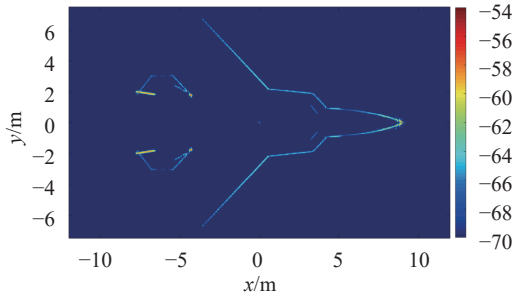

Fig. 16 Results of ISAR image of SC model with improved parameters

7. Conclusions

Taking the typical stealth target as an example, this paper analyzes the differences in the scattering characteristics between the LDT and a nonstealth target. The visible SC of stealth aircraft under a sensitive observation angle is usually weak and tightly distributed, which makes it difficult to locate the SCs and extract their parameters from the scattering field. To address this, this paper presents improved SC models according to the scattering characteristics of LDTs. The high-precision SC model is established by employing the induced current intensity distribution combined with joint time-frequency analysis and the improved parameter estimation method.

Although the SC model is established from a scattered field collected at a single frequency, it can be employed to simulate broadband radar imaging. It is confirmed that the signatures in the HRRP and ISAR images simulated by the SC model agree well with those simulated by the full-wave method. The improved SC model of the LTDs can provide support for radar identification and tracking of stealth targets.

References

[1] Editorial board of special issue for “computational electromagnetics”. Ten problems in computational electromagnetics. Chinese Journal of Radio Science, 2020, 35(1): 3–12. (in Chinese)

[2] DING B Y, WEN G J, HUANG X H, et al. Target recognition in synthetic aperture radar images via matching of attributed scattering centers. IEEE Journal of Selected Topics in Applied Earth Observations and Remote Sensing, 2017, 10(7): 3334–3347.

[3] LI T L, DU L. Target discrimination for SAR ATR based on scattering center feature and k-center one-class classification. IEEE Sensors Journal, 2018, 18(6): 2453–2461.

[4] LIU M, CHEN S C, WU J, et al. SAR target configuration recognition via two-stage sparse structure representation. IEEE Trans. on Geoscience and Remote Sensing, 2018, 56(4): 2220–22325.

[5] MILLER E K, LAGER D L. Inversion of one-dimensional scattering data using Prony’s method. Radio Science, 1982, 17(1): 211–217.

[6] POTTER L C, CHIANG D M, CARRIERE R, et al. A GTD-based parametric model for radar scattering. IEEE Trans. on Antennas and Propagation, 1995, 43(10): 1058–1067.

[7] GERRY M J, POTTER L C, GUPTA I J, et al. A parametric model for synthetic aperture radar measurements. IEEE Trans. on Antennas and Propagation, 1999, 47(7): 1179–1188.

[8] HE Y, HE S Y, ZHANG Y H, et al. A forward approach to establish parametric scattering center models for known complex radar targets applied to SAR ATR. IEEE Trans. on Antennas and Propagation, 2014, 62: 6192–6205.

[9] XIAO G L, GUO K L, WU B Y, et al. Accurate scattering centers modeling for complex conducting targets based on induced currents. Science China (Information Sciences), 2021, 64(2): 268–270.

[10] ERER I, GULTEKIN O, GUNEL T. Data extrapolation based CLEAN algorithm for one dimensional scattering center

extraction. Proc. of the IEEE 14th Signal Processing and Communications Applications, 2006. DOI:10.1109/SIU.2006.1659774.
[11] CHEN X, TIAN Y G, DONG C Z, et al. An improved state space approach based method for extracting the target scattering center. Proc. of the International Applied Computational Electromagnetics Society Symposium, 2017. DOI: 10.1007/s11432-010-4137-Z.
[12] WEI S M, WANG J, SUN J P, et al. Estimation of UWB radar scattering center with GTD-based 2D state-space method. Proc. of the IEEE 10th International Conference on Signal Processing, 2010: 2270–2273.
[13] LI Q F, GUO K Y, ZHAI Y. Performance comparsion among different objective functions in paramter estimation of scattering center. Proc. of the International Applied Computational Electromagnetics Society Symposium, 2017: 8051928.
[14] ZHANG S B, JI T T, WANG W Y, et al. Application of PSO-GA & CGA in sea-clutter Doppler spectrum modeling. Proc. of the International Joint Conference on Neural Networks, 2020, 1-8. DOI: 10.1109/IJCNN48605.2020.9207683.
[15] DONELLI M, FRANCESCHINI G, MARTINI A, et al. An integrated multiscaling strategy based on a particle swarm algorithm for inverse scattering problems. IEEE Trans. on Geoscience and Remote Sensing, 2006, 44(2): 298–312.
[16] YANG M L, WU B Y, GAO H W, et al. A ternary parallelization approach of MLFMA for solving electromagnetic scattering problems with over 10 billion unknowns. IEEE Trans. on Antennas and Propagation, 2019, 67(11): 6965–6978.
[17] HE S S. The analysis of nonideal scattering phenomena in radar imaging. Changsha: National University of Defense Technology, 2005.
[18] GUO K Y, QU Q Y, SHENG X Q. Geometry reconstruction based on attributes of scattering centers by using time-frequency representations. IEEE Trans. on Antennas and Propagation, 2016, 64(2): 708–720.
[19] LIU H Y, TIAN G, SHI Z J. The comparison of time-frequency analysis methods and their applications. Computerized Tomography Theory and Applications, 2015, 24(2): 199–208.
[20] TAEBI A, MANSY H A. Analysis of seismocardiographic signals using polynomial chirplet transform and smoothed pseudo Wigner-Ville distribution. Proc. of the IEEE Signal Processing in Medicine and Biology Symposium, 2017. DOI: 10.1109/SPMB.2017.8257022.
[21] CHEN V C, QIAN S. CFAR detection and extraction of unknown signal in noise with time-frequency Gabor transform. Proc. of SPIE-The International Society for Optical Engineering, 1996: 285–294.
[22] PEI S C, HUANG S G. Adaptive STFT with chirp-modulated Gaussian window. Proc. of the IEEE International Conference on Acoustics, Speech and Signal Processing, 2018: 4354–4358.
[23] VETTERLI M, HERLEY C. Wavelets and filter banks: theory and design. IEEE Trans. on Signal Processing, 1992, 40(9): 2207–2232.
[24] XIN N, WANG G H, ZHANG J. A synthetical pose estimation of SAR imagery using Hough transform and 2-D continuous wavelet transform. Proc. of the CIE International Conference on Radar, 2006. DOI: 10.1109/ICR.2006.343503.
[25] GILLES J. Empirical wavelet transform. IEEE Trans. on Signal Processing, 2013, 61(16): 3999–4010.
[26] NING J, PENG J G. Repression of the cross-term interference based on Emd and Cohen's class distribution. Proc. of the IEEE Circuits and Systems International Conference on Testing and Diagnosis, 2009. DOI: 10.1109/CAS-ICTD.2009.4960861.
[27] MERLIN T, ROSHEN J, LETHAKUMARY B. Comparison of WVD based time-frequency distributions. Proc. of the International Conference on Power, Signals, Controls and Computation, 2012. DOI: 10.1109/EPSCICON.2012.6175242.
[28] ZHAO X T, GUO K, SHENG X. Scattering center model for edge diffraction based on EEC formula. Proc. of the Progress in Electromagnetic Research Symposium, 2016: 286–290.
[29] MILLER E K. A discussion and survey of model-based parameter estimation in computational electromagnetics. Proc. of the IEEE Antennas and Propagation Society International Symposium, 1997, 3: 1980–1983.
[30] ZHAO X T, GUO K, SHENG X. Modifications on parametric models for distributed scattering centres on surfaces with arbitrary shapes. IET Radar, Sonar & Navigation, 2019, 13: 2174–2182.
[31] GORDEN W B. Far-field approximations to the Kirchoff-Helmholtz representations of scattered fields. IEEE Trans. on Antennas and Propagation, 1975, 23(4): 590–592.
[32] MORAN M B H, CUNO J S, RIVEAUX J A, et al. Automatic sinusoidal curves detection in borehole images using the iterated local search algorithm. Proc. of the International Conference on Systems, Signals and Image Processing, 2020: 255–260.

Biographies

CHEN Yanxi was born in 1994. He received his B.S. degree from Beijing Institute of Technology, Beijing, China, in 2017. He is currently a Ph.D. degree candidate in Beijing Institute of Technology. His major research interests include radar scattering center and electromagnetic simulation and application.
E-mail: cyx_bit@126.com

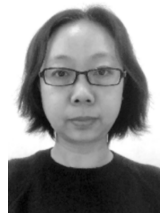

GUO Kunyi was born in 1976. She received her Ph.D. degree from Chinese Academy of Sciences, Beijing, China, in 2005. She is currently a professor with the School of Information and Electronics, Beijing Institute of Technology, Beijing. Her current research interests include electromagnetic scattering, antenna propagation, scattering center modeling, and radar signal processing.
E-mail: guokunyi@bit.edu.cn

XIAO Guangliang was born in 1992. He received his B.S. degree from Beijing Institute of Technology in 2016. He is currently a Ph.D. degree candidate in Beijing Institute of Technology. His major research interests include radar target character and electromagnetic simulation and application.
E-mail: 20111462@bit.edu.cn

SHENG Xinqing was born in 1968. He received his B.S., M.S., and Ph.D. degrees from University of Science and Technology of China, Hefei, China, in 1991, 1994, and 1996, respectively. He is currently a chair professor of the School of Information and Electronic, Beijing Institute of Technology, Beijing, China. His current research interests include computational electromagnetics, target electromagnetic characteristics and stealth design, and complex electromagnetic environment simulation.
E-mail: xsheng@bit.edu.cn